Integration of the guiding-center equations in toroidal fields utilizing a local linearization approach

Michael Eder

PPPL, Theory seminar, 17 June 2021

Outline

Outline

Motivation: A new orbit integration method

1. **Physically correct long time orbit dynamics**
2. **Low sensitivity to noise in fields**
3. **Efficient box counting**
4. **Computational efficiency**

$\rightarrow$ **Long-term goal:**
Kinetic modelling of distribution function moments

Local Linearization Approach

- **Linearization:** Piecewise linear toroidal electromagnetic fields
- **Mesh-based:** 3D tetrahedral cells
- **Quasi-geometric**:
  - Formulation preserves non-canonical symplectic form
  - Series expansion in time-like orbit parameter
- **Fortran code:**
  - **GORILLA**: **G**uiding-center **OR**bit **I**ntegration with **L**ocal **L**inearization **A**pproach

Outline

Guiding-center approx. for charged particle orbit

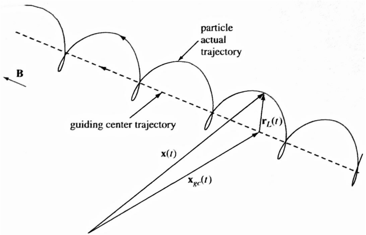

Fundamentals of Plasma Physics,
Dr. Paul Bellan, Cambridge Press 2006

- Lagrangian for charged-particle motion in an electromagnetic field:

$$\mathcal{L}\left(\mathbf{x}, \dot{\mathbf{x}}; t\right) = \frac{m}{2}\left|\dot{\mathbf{x}}\right|^2 + \frac{e}{c}\dot{\mathbf{x}} \cdot \mathbf{A}\left(\mathbf{x}, t\right) - e\Phi\left(\mathbf{x}, t\right) \quad (1)$$

- Particle position via guiding-center

$$\mathbf{x} \equiv \mathbf{x}_{gc} + \rho \quad (2)$$

- Guiding-center phase-space Lagrangian:[1]

$$\mathcal{L}_{gc}\left(\mathbf{x}_{gc}, J_\perp, \phi, w\right) = \left[\frac{e}{c}\mathbf{A}\left(\mathbf{x}_{gc}\right) + m v_{\|}\left(\mathbf{x}_{gc}, J_\perp, w\right)\frac{\mathbf{B}\left(\mathbf{x}_{gc}\right)}{B\left(\mathbf{x}_{gc}\right)}\right] \cdot \dot{\mathbf{x}}_{gc} - J_\perp \dot{\phi} - w \quad (3)$$

[1] Littlejohn 1983; Cary and Brizard 2009.

Formulation of orbit integration method

- Use the Hamiltonian form of guiding center equations[2] in curvilinear coordinates,

$$\dot{x}^i = \frac{v_\parallel \varepsilon^{ijk}}{\sqrt{g} B_\parallel^*} \frac{\partial A_k^*}{\partial x^j}, \qquad A_k^* = A_k + \frac{v_\parallel}{\omega_c} B_k, \tag{4}$$

$$v_\parallel = \sigma \left(\frac{2}{m_\alpha} \left(w - J_\perp \omega_c - e_\alpha \Phi \right) \right)^{1/2}, \tag{5}$$

$$\frac{v_\parallel^2}{2} = U, \qquad U = U(x^j). \tag{6}$$

- Treat $v_\parallel$ as an independent variable
- Replace time with orbit parameter τ: $\mathrm{d}t = \sqrt{g} B_\parallel^* \mathrm{d}\tau$

[2] Boozer 1980; Littlejohn 1983.

Formulation of orbit integration method

- Set of four equations:

$$\begin{aligned} B^*_\parallel \sqrt{g}\dot{x}^i = \frac{\mathrm{d}x^i}{\mathrm{d}\tau} &= \varepsilon^{ijk}\left(v_\parallel \frac{\partial A_k}{\partial x^j} + 2U\frac{\partial}{\partial x^j}\frac{B_k}{\omega_c} + \frac{B_k}{\omega_c}\frac{\partial U}{\partial x^j}\right) \\ B^*_\parallel \sqrt{g}\dot{v}_\parallel = \frac{\mathrm{d}v_\parallel}{\mathrm{d}\tau} &= \varepsilon^{ijk}\frac{\partial U}{\partial x^i}\left(\frac{\partial A_k}{\partial x^j} + v_\parallel \frac{\partial}{\partial x^j}\frac{B_k}{\omega_c}\right) \end{aligned} \tag{7}$$

- Approximate $A_k, B_k/\omega_c$, ω_c and Φ by linear functions in spatial cells:

$$\boxed{\frac{\mathrm{d}z^i}{\mathrm{d}\tau} = a^i_k z^k + b^i} \tag{8}$$

$$\begin{aligned} z^i &= x^i \quad \text{for} \quad i = 1,2,3 \\ z^4 &= v_\parallel \end{aligned}$$

3D field aligned grid: tetrahedral cells I

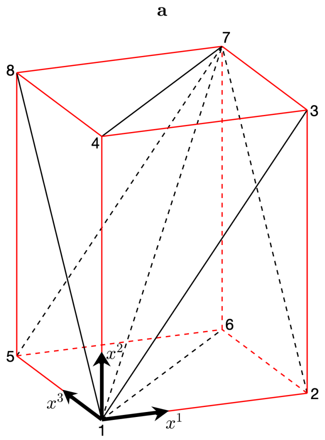

(x^1, x^2, x^3) is aligned to coordinate system.
E.g., $(x^1, x^2, x^3) = (s, \vartheta, \varphi)$ or (R, φ, Z)

3D field aligned grid: tetrahedral cells II

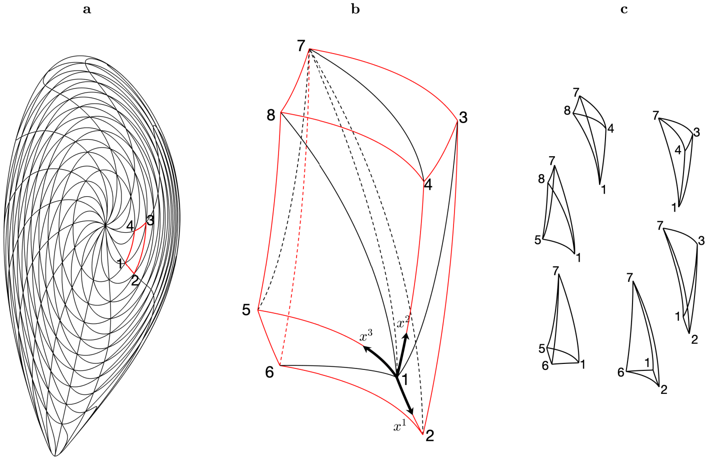

Aligned to symmetry flux coordinates: $(x^1, x^2, x^3) = (s, \vartheta, \varphi)$

Physically correct long time orbit dynamics

- Linear approximation of field quantities does **not destroy the Hamiltonian nature** of the original guiding center equations.
- Non-canonical Hamiltonian form of linear ODE set

$$\frac{\mathrm{d}z^i}{\mathrm{d}\tau} = \Lambda^{ij}\frac{\partial H}{\partial z^j}, \qquad \Lambda^{ij}(\mathbf{z}) = \left\{z^i, z^j\right\}_\tau, \tag{9}$$

with Hamiltonian $H(\mathbf{z}) = v_\parallel^2/2 - U(\mathbf{x})$ and antisymmetric Poisson matrix $\Lambda^{ij}(\mathbf{z})$.

Physically correct long time orbit dynamics

- Liouville's theorem is fulfilled
  - Coordinate set:

$$\mathbf{y} = (\mathbf{x}, J_\perp, \phi, v_\parallel)$$

  - Phase space Jacobian[3]:

$$J = \frac{\partial(\mathbf{r}, \mathbf{p})}{\partial(\mathbf{x}, J_\perp, \phi, v_\parallel)} = \frac{m_\alpha e_\alpha}{c} \sqrt{g} B_\parallel^*$$

  - Divergence of the phase space flow velocity:

$$\frac{1}{J} \frac{\partial \left(J \dot{y}^i \right)}{\partial y^i} \equiv 0$$

  - Relation holds for piecewise linear approximation.

[3] Littlejohn 1983.

Properties of orbit integration method

- **Physically correct long time orbit dynamics**
  - preserved total energy
  - preserved magnetic moment
  - preserved phase space volume
- **Computationally efficient**
  - relaxed requirement to orbit shape
  - lowest order approximation for time evolution
  - locally linear ODE set with constant coefficients
- **Insensitive to noise in fields**

Outline

Numerical solution

- Locally linear ODE set:

$$\frac{\mathrm{d}\mathbf{z}(\tau)}{\mathrm{d}\tau} = \hat{\mathbf{a}} \cdot \mathbf{z} + \mathbf{b}$$

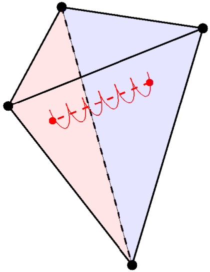

- $\hat{\mathbf{a}}$ and $\mathbf{b}$ are **constant** inside cells.
- Formal solution:

$$\mathbf{z}(\tau) = \mathbf{z}_0 + \sum_{k=1}^{K} \frac{\tau^k}{k!} \left(\hat{\mathbf{a}}^{k-1} \cdot \mathbf{b} + \hat{\mathbf{a}}^k \cdot \mathbf{z}_0 \right) \tag{10}$$

- Exact for $K \to \infty$

Orbit intersections with tetrahedra faces

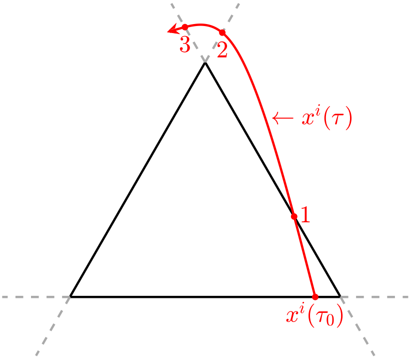

$$\mathbf{z}(\tau) = \mathbf{z}_0 + \sum_{k=1}^{K} \frac{\tau^k}{k!} \left(\hat{\mathbf{a}}^{k-1} \cdot \mathbf{b} + \hat{\mathbf{a}}^k \cdot \mathbf{z}_0\right)$$

$$\downarrow$$

$$F^\alpha(\mathbf{z}) \equiv n_i^{(\alpha)} \left(x^i - x^i_{(\alpha)}\right) = 0$$

$$\downarrow$$

$$\mathbf{n}^\alpha \cdot \left(\mathbf{z}_0 + \sum_{k=1}^{K} \frac{\tau_e^k}{k!} \left(\hat{\mathbf{a}}^{k-1} \cdot \mathbf{b} + \hat{\mathbf{a}}^k \cdot \mathbf{z}_0\right) - \mathbf{z}^\alpha\right) = 0$$

3D tetrahedral cell is depicted as a **2D triangle** in the interest of simplification.

Runge-Kutta vs. Polynomials

Runge-Kutta (GORILLA RK4):

- The ODE set is numerically solved via **Runge-Kutta 4** in an iterative scheme.
- Iterative scheme uses **Newton's method** and a quadratic analytic estimation for the initial step length.

Analytic Polynomial (GORILLA Poly):

- Truncation of series at $K = 2, 3, 4$
- Algebraic equations: approximate solutions of various orders in Larmor radius.

Dwell time & integrals of velocity powers

- Dwell time of particle inside spatial cell
- Analytic formulation of parallel velocity

$$v_{\|}(\tau) = e^{\alpha \tau} \left(v_{\|,0} + \frac{\beta}{\alpha} \right) \frac{\beta}{\alpha}$$

- Analytic formulation of velocity power integrals of $v_{\|}, v_{\|}^2$ and $v_{\perp}^2$

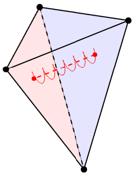

Advantage:
Straightforward computation of spatial distributions within Monte Carlo procedures.

Outline

Poincare plots of guiding center orbits

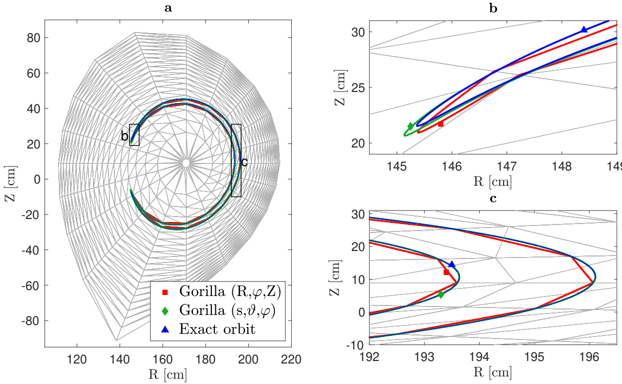

- Quasi-geometric integration: Not exact orbit shape.
- Axisymmetric (2D): Canonical toroidal angular momentum is preserved. ($N_{\text{mappings}} = 10^7$)

Canonical toroidal angular momentum p_φ

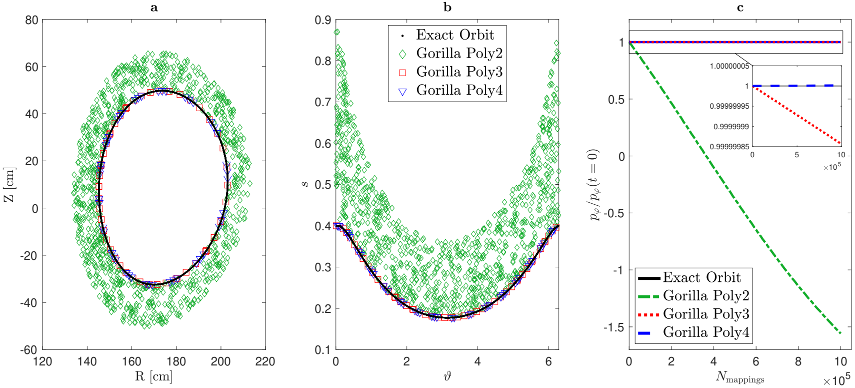

- Passing high energy ion with 300 keV
- Polynomial order $K = 2, 3, 4$ and exact orbit (RK 4/5)

Axisymmetric noise of electrostatic and vector potential

$$\xi = 0 \ldots 1, \quad \text{e.g. } \Phi^{\text{noisy}} = \Phi(1 + \epsilon_\Phi \xi)$$

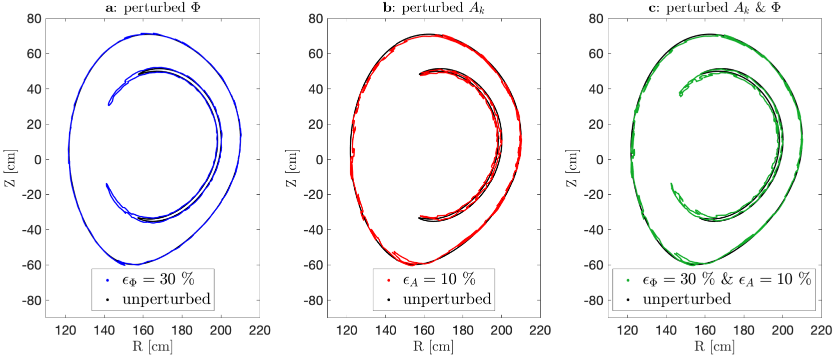

- Similar orbit shape (compared to unperturbed orbit)
- Canonical toroidal angular momentum is preserved.

Outline

Artifact: Numerical field line diffusion

- **Test case:** 2D field with harmonic perturbation of vector potential

$$A_\varphi = \psi_{\mathrm{pol}}(s)(1 + \varepsilon_M \cos(m_0\vartheta + n_0\varphi)). \tag{11}$$

- Due to the linearization of fields for 3D configurations, **KAM surfaces can be destroyed**.
  $\rightarrow$ **ergodic passing particle orbit**
- Numerical diffusion is below the level of classical electron diffusion (perturbed tokamak)
  $\rightarrow$ **Diffusion can be safely ignored.**

Artifact: Numerical field line diffusion

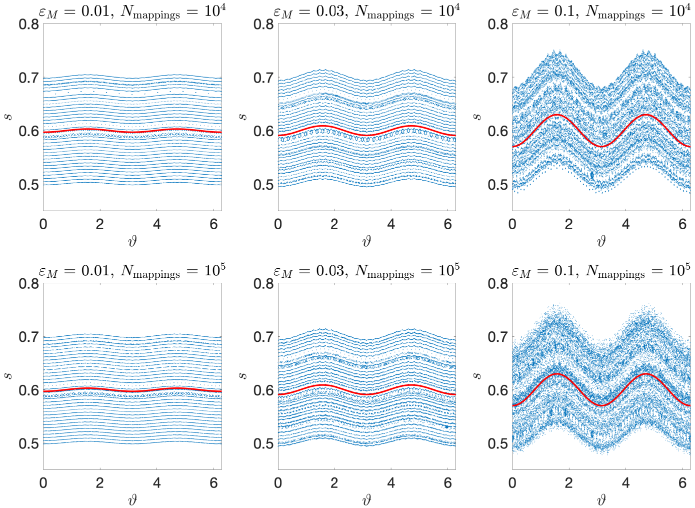

Poincaré plots of field lines

GORILLA Poly:
34 equidistant flux surfaces
$N_\vartheta = N_\varphi = 30$
$K = 2$

Solid red line shows a cross-section of one exact corrugated flux surface.

Stellarator field: Poincaré projection

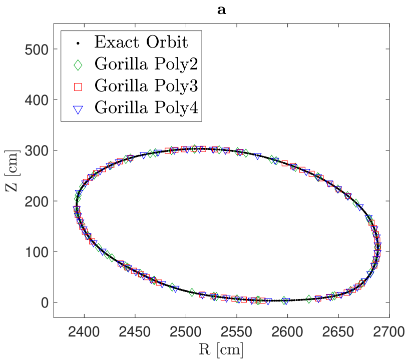

- Trapped ion with 3 keV
- Poloidal projection at $v_{\|} = 0$ switching sign from - to +

Stellarator field: Parallel adiabatic invariant $J_\parallel$

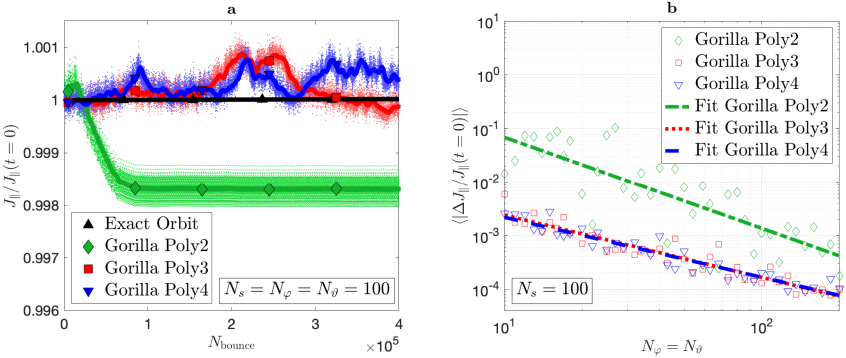

- Violation of Hamiltonian structure for $K = 2$ (attractor)
- Convergence with grid size: $J_\parallel$ averaged over 10^5 bounce times (in **b**)

Outline

Mono-energetic radial diffusion coefficient D_{11}

- D_{11} as a function of collisionality ν^* is evaluated with standard Monte Carlo method.[4] (10 000 test particles)

$$D_{11} = \frac{1}{2t}\langle (s(t) - s_0)^2 \rangle. \tag{12}$$

- Collisions are realized by pitch angle scattering (Lorentz scattering operator).
- Normalization:

$$\begin{aligned} \nu^* &= \frac{R_0 \nu_c}{\iota v} \qquad \text{(collisionality)} \\ v_E^* &= \frac{c E_r}{v B_0} \qquad \text{(Mach number)} \end{aligned}$$

[4] Boozer and Kuo-Petravic 1981.

Mono-energetic radial diffusion coefficient D_{11}

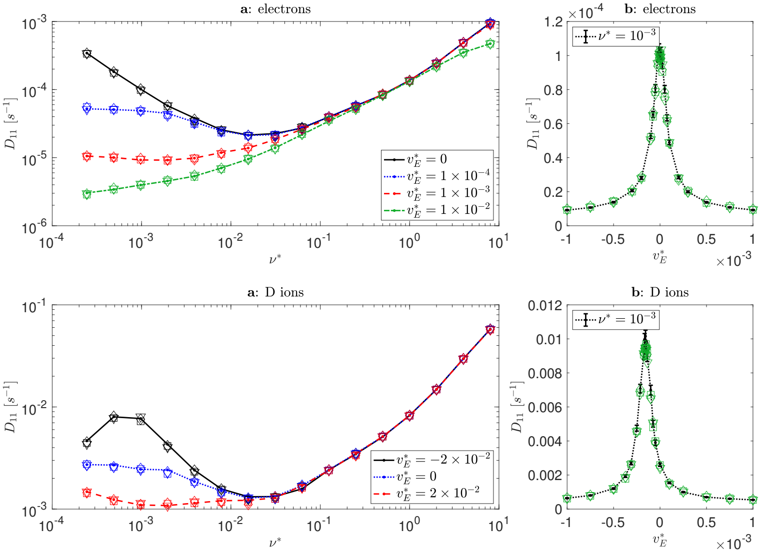

Reference computation: Lines of various styles (see the legends)

GORILLA Poly: Markers: $K = 2$ ($\Diamond$), $K = 3$ ($\Box$) and $K = 4$ ($\triangledown$)

Error bars indicate 95 % confidence interval.

CPU benchmark

- Accuracy vs. efficiency
  - **Accuracy:** Relative error of D_{11}
  - **Efficiency:** Relative CPU time for pure orbit integration

Boundary conditions:

- Fixed collisionality $\nu^* = 10^{-3}$ and Mach number $v_E^* = 10^{-3}$
- Number of test particles: 30 000
- Reference integrators:
  - adaptive Runge-Kutta 4/5 (rel. tolerance = 10^{-9})
  - Runge-Kutta 4

CPU benchmark for D_{11}

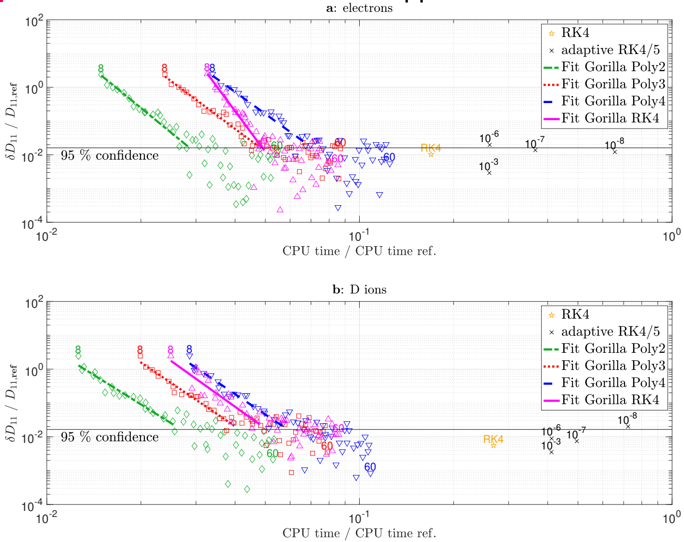

Reference computation: adaptive Runge-Kutta 4/5 (rel. tol. = 10^{-9})

Compared integrators: adaptive RK 4/5 ($\times$) (various rel. tol.)

Runge-Kutta 4: ($\star$)

GORILLA Poly: $K = 2$ ($\Diamond$), $K = 3$ ($\square$) and $K = 4$ ($\triangledown$)

GORILLA RK4: ($\triangle$)

GORILLA: Angular grid size $N_\vartheta \times N_\varphi$ varied from 8×8 to 60×60.

Outline

Confined fraction f_c of 3.5 MeV fusion alphas

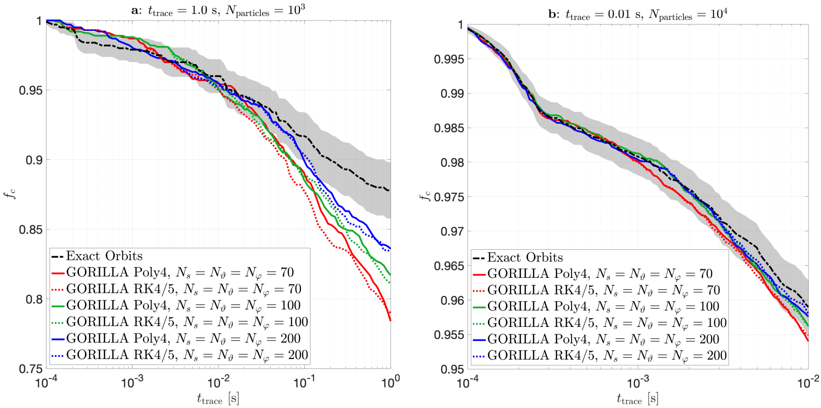

- Numerical diffusion (due to linearization) strongly scales with Larmor radius.
- Numerical diffusion affects confined fraction f_c.

Relative error of f_c @ t = 0.01 s vs. grid size

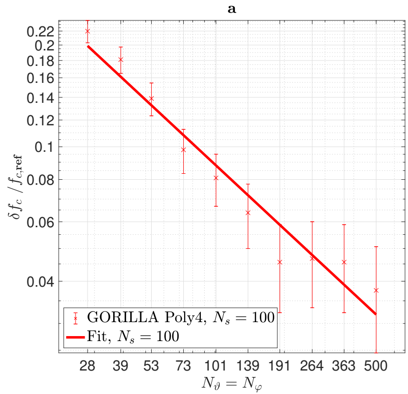

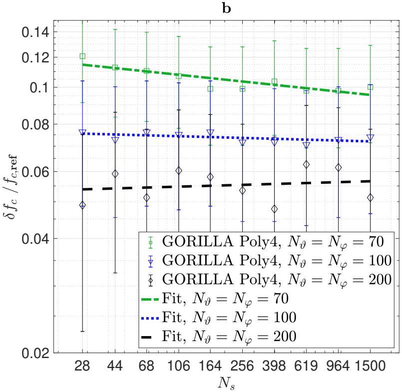

- Numerical diffusion scales inversely with angular grid size
- Numerical diffusion is (almost) not affected by radial grid size

CPU benchmark for f_c

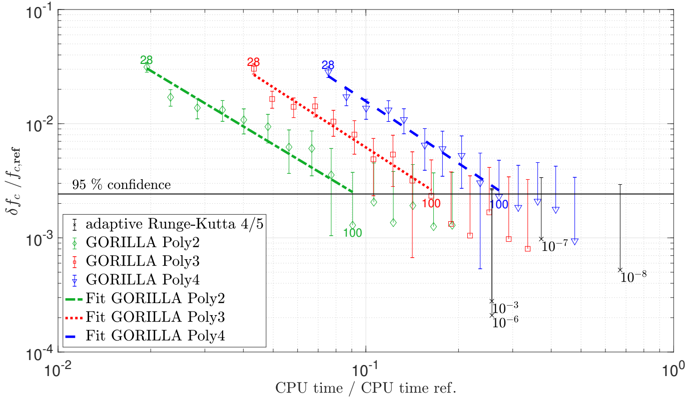

Reference computation: adaptive Runge-Kutta 4/5 (rel. tol. = 10^{-9})

Compared integrators: adaptive RK 4/5 ($\times$) (various rel. tol.)

GORILLA Poly: $K = 2$ ($\Diamond$), $K = 3$ ($\square$) and $K = 4$ ($\triangledown$)

GORILLA: Angular grid size $N_\vartheta \times N_\varphi$ varied from 28×28 to 200×200.

Outline

Benefits of the integration method

- **Computational efficiency** (up to **10x** faster than RK4)
- **Physically correct** long time orbit dynamics
  - preserved total energy
  - preserved magnetic moment
  - preserved phase space volume
- Formulation in **general curvilinear coordinates**
- **Low sensitivity** to noise in electromagnetic fields
- Straightforward computation of **spatial distributions** within **Monte Carlo** procedures
  - dwell time and velocity power integrals in spatial cells

Limitations of the integration method

- Implemented only for **(quasi-)static electromagnetic fields**
- **Artificial chaotic diffusion** in 3D fields
  - **Magnetic flux coordinates** strongly reduce chaos.
    - Chaotic diffusion strongly scales with **Larmor radius**.
    - Chaotic diffusion inversely scales with **angular grid size**.
  - **Thermal particles**: Negligibly small through moderate grid refinement.
  - **Fusion alphas**: Chaotic diffusion affects confined fraction.

Outlook & proposed project

- Global Monte Carlo computations of parallel equilibrium **current density**, **charge density** and **pressure tensor** distributions
- Implementation of correct time dynamics

$$\frac{\mathrm{d}t}{\mathrm{d}\tau} = \left(\sqrt{g}B_{\|}^{*}\right)^{(L)}$$

→ **Fast** drift-kinetic **electron** solver for **PIC** codes, e.g. XGC

Thank you for your attention!

Documentation & Code:

- Eder et *al.*, Physics of Plasmas **27**, 122508 (2020)
  https://doi.org/10.1063/5.0022117
- Fortran code available on GitHub
  https://github.com/itpplasma/GORILLA
  Publication planned at Journal of Open Source Software

Bibliography I

Boozer, Allen H. (May 1980). **Guiding center drift equations**. *The Physics of Fluids* 23.5, pp. 904–908. ISSN: 0031-9171. DOI: 10.1063/1.863080. URL: https://aip.scitation.org/doi/10.1063/1.863080 (visited on 04/29/2020).

Boozer, Allen H. and Gioietta Kuo-Petravic (May 1981). **Monte Carlo evaluation of transport coefficients**. *The Physics of Fluids* 24.5, pp. 851–859. ISSN: 0031-9171. DOI: 10.1063/1.863445. URL: https://aip.scitation.org/doi/10.1063/1.863445 (visited on 04/29/2020).

Cary, John R. and Alain J. Brizard (May 2009). **Hamiltonian theory of guiding-center motion**. en. *Reviews of Modern Physics* 81.2, pp. 693–738. ISSN: 0034-6861, 1539-0756. DOI: 10.1103/RevModPhys.81.693. URL: https://link.aps.org/doi/10.1103/RevModPhys.81.693 (visited on 08/17/2020).

Bibliography II

Littlejohn, Robert G. (Feb. 1983). **Variational principles of guiding centre motion**. en. *Journal of Plasma Physics* 29.1, pp. 111–125. ISSN: 1469-7807, 0022-3778. DOI: 10.1017/S002237780000060X. URL: https://www.cambridge.org/core/journals/journal-of-plasma-physics/article/variational-principles-of-guiding-centre-motion/8FF3F0D2C6ECB02E983AE506DC40684F (visited on 04/29/2020).